ISSN (Print) 1226-1750
ISSN (Online) 2233-6656
Journal of Magnetics 30(4), 498-509 (2025) https://doi.org/10.4283/JMAG.2025.30.4.498

Design and Simulation of Two-Degree-of-Freedom Voice Coil Spherical Motor with Magneto Restoring Torque

Wen-Shao Huang[1] and Chien-Sheng Liu[1,2]*

[1]*Department of Mechanical Engineering, National Cheng Kung University, Taiwan, No.1, University Road, Tainan City 70101, Taiwan*
[2]*Academy of Innovative Semiconductor and Sustainable Manufacturing, National Cheng Kung University, Taiwan, No.1, University Road, Tainan City 70101, Taiwan*

(Received 29 December 2024, Received in final form 9 December 2025, Accepted 9 December 2025)

Through extensive research and practical validation, the spherical motor has progressed from a conceptual idea to a promising candidate for future applications in motor design. Among these developments, several voice coil spherical motor designs have been proposed. However, the lack of application studies for these designs highlights opportunities for further improvement. This study introduces a novel magnetic circuit design based on the principles and theories of traditional voice coil motors. By arranging the magnets' N-poles in a bidirectional configuration, the design enables both sides of a single coil to generate Lorentz force in the same direction. Furthermore, the combination of yoke iron and magnet geometry provides a magnetic restoring force, maintaining horizontal alignment when the motor is not energized, thereby enhancing controllability. Electromagnetic simulations of the proposed magnetic circuit structure were conducted using ANSYS Maxwell, demonstrating improved output force compared to previously published designs.

Keywords: spherical motor, spherical actuator, voice coil actuator, magnetic restoring torque, lorentz force, voice coil spherical motor

1. Introduction

Conventional multi-degree-of-freedom (MDOF) output devices are composed of a combination of multiple actuators, which can result in mechanical issues such as backlash or center position errors. To address these challenges, the spherical motor was proposed. By driving a single rotor to achieve up to 3DOF in rotation, the spherical motor offers advantages such as reduced mechanical error accumulation, overlapping centroids, and a direct-drive mechanism. As a result, spherical motors are expected to deliver higher precision, improved responsiveness, and a simplified kinematic chain.

To date, numerous spherical motor designs have been proposed. Based on their driving methods, spherical motors can be classified into five types: permanent magnet spherical motors [1-6], induction spherical motors [7-10], reluctance spherical motors [11-13], piezoelectric spherical motors [14-16], and voice coil spherical motors [17-23]. Among these, voice coil spherical motors have an advantage in positioning due to their driving force—Lorentz force—which provides a linear relationship between force output and current. By enhancing the precision positioning capabilities of spherical motors, voice coil spherical motors have the potential to outperform other types.

After reviewing several proposed voice coil spherical motor designs [17-22], this study introduces a new two-degree-of-freedom voice coil spherical motor design, verified through Maxwell 3D simulations. Although 3-DOF spherical motors possess numerous advantages, the 2-DOF tilting motion is enough for many critical applications, such as optical mirror sets or precision pointing systems. Therefore, this study first focuses on a 2-DOF structure, which allows for a more concentrated analysis and optimization of the proposed novel magnetic circuit, especially its characteristic of generating a linear restoring torque. The design methodology and simulation results validated in this paper are not only applicable to 2-DOF applications but also lay a solid foundation for the possibility of extending this magnetic circuit design to 3-DOF in the future. The results demonstrate that this

*Corresponding author: Tel: +886-6-2757575 (ext. 62100)
Fax: +886-6-2352973, e-mail: csliu@mail.ncku.edu.tw

design, with a maximum working angle of ±30 degrees, features a highly linear restoring torque that maintains the rotor in a level position when no current is applied. It also exhibits a small rate of change in output torque with respect to rotor angle and enables independent rotational movement along the X and Y axes. These features suggest that the proposed design holds promise for improved position control.

2. Magnetic Circuit Design of Proposed Spherical Motor

The magnetic circuit design of the proposed spherical motor is illustrated in Fig. 1. The selected area is designated as the stator structure, while the remaining structure serves as the rotor. The yoke structure within the black box generates a magnetic restoring force, while the coil within the red box produces Lorentz force when current flows through it. This force drives any attached components to move in the direction of the Lorentz force. The remaining components ensure that the magnetic field forms a closed loop. For better clarity, the yoke structures in the black box, which produce restoring force, are referred to as "restorative yoke structures." The generation mechanism of this magnetic restoring torque originates from the Magnetic Reluctance Force, also known as the minimum reluctance principle. The permanent magnets and the 'restorative yoke structures' form a magnetic circuit.

When the rotor is at the 0-degree level position, the magnetic flux passes symmetrically through the restorative yoke structures on both sides. In this state, the air gap of this circuit is minimized, resulting in the lowest possible magnetic reluctance. However, when the rotor tilts, this symmetry is broken. This changes the air gap geometry and increases the total magnetic reluctance. According to the minimum reluctance principle, the magnetic field will exert a force (manifesting as a torque) to pull the rotor back toward the position of minimum reluctance—the 0-degree equilibrium point. This effect acts as a passive magnetic spring, providing the restoring torque that automatically centers the motor. This passive effect acts as a magnetic spring. As the simulation results later demonstrate (Section 6), this restoring torque exhibits a highly linear relationship with the tilt angle θ, which can be modeled as:

$$\tau_r(\theta) \approx -K_r \cdot \theta \tag{1}$$

where K_r is the rotational stiffness of the magnetic spring.

If the height of the restorative yoke structure is increased, as illustrated in Fig. 2(a), it now allows greater magnetic flux to flow through. This results in a stronger magnetic force, as magnetic force increases with higher magnetic flux. Similarly, for the red box area, increasing the height of the coil structures, as shown in Fig. 2(b), allows for more coil turns within the structure. With the designed orientation of the permanent magnets, the increased-height coil structure continues to intersect the magnetic field effectively. Consequently, when the same current is applied, the increased-height coil structure permits a greater current flow, generating a stronger Lorentz force compared to a structure with no height increase.

In summary, this magnetic circuit design incorporates coil structures and restorative yoke structures, which are positioned together, separate from the main frame of the structure with the permanent magnet. This assembly is referred to as the mover. Within the mover, the height of the restorative yoke structure determines the magnitude of the magnetic restoring force acting on it. A greater height of the restorative yoke structure results in a stronger magnetic force when the mover is at the same position away from the centerline of the main frame. Additionally, the height of the coil structure allows for more current to flow through the magnetic field, thereby generating a greater Lorentz force on the mover.

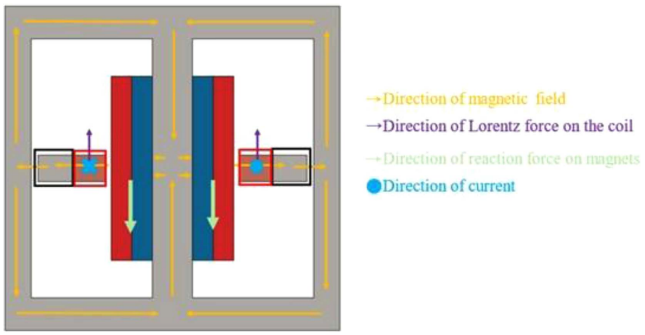

Fig. 1. (Color online) Magnetic circuit of proposed design.

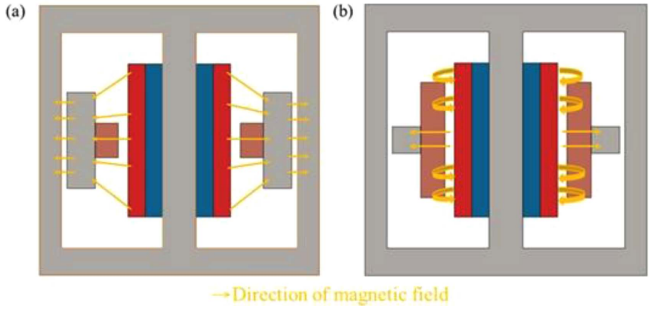

Fig. 2. (Color online) (a) Increased restorative yoke structure (b) increased height of coil structure.

3. 2DOF Spherical Motor Model Design

Based on the magnetic circuit design, three variants of a two-degree-of-freedom voice coil spherical motor structure were developed as 3D models for magnetic simulation. The spherical motor structure is illustrated in Fig. 3. Fig. 3(a) shows a cross-section of a single magnetic circuit structure. With four magnetic circuit structures in total, two pairs of circuits are combined, each pair providing one degree of rotational output. The magnetic circuit of one pair is illustrated in Fig. 3(b).

In the control method of the proposed spherical motor, when current is applied in the direction illustrated in Fig. 4, with the coil and restorative yoke structure fixed, the structures containing the permanent magnets will rotate counterclockwise due to the reaction force produced by the Lorentz force. Following the same control principle, applying current in the opposite direction will cause the permanent magnet structure to rotate clockwise. This design is expected to ensure that rotation along one axis does not affect the other axes, eliminating the need to account for interactions when other axes are not in a level position.

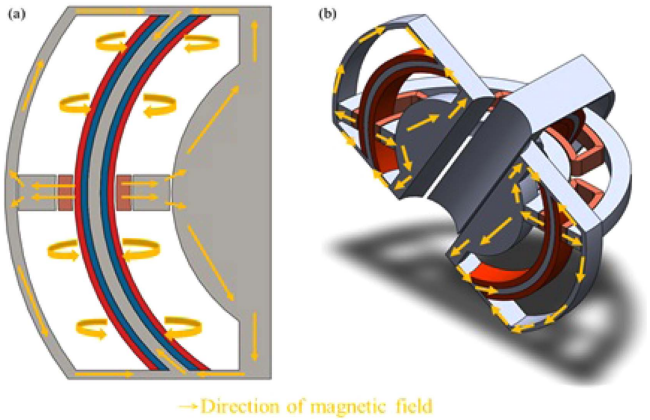

Fig. 3. (Color online) (a) Magnetic circuit illustration for single structure (b) magnetic circuit illustration for section of spherical motor structure.

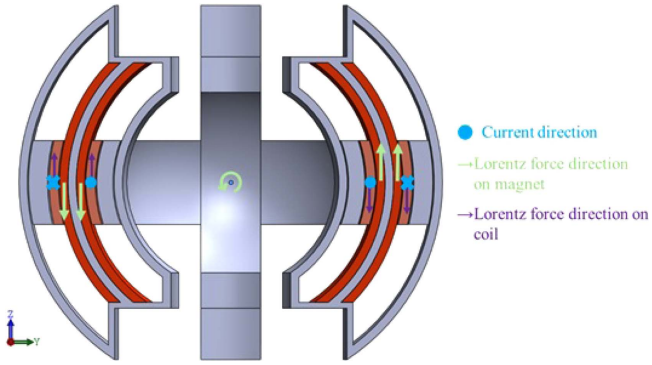

Fig. 4. (Color online) Working Principle of proposed spherical motor.

To verify the effectiveness of the coil and restorative yoke structure design as illustrated in the magnetic circuit design, three variants of the model were developed, as shown in Figs. 5, 6, and 7. In Fig. 5, the model features the shortest height for both the coil and restorative yoke structures, as shown in Fig. 5(a).

Based on the principles outlined in Section 2, this configuration possesses the shortest restorative yoke structure, which provides the smallest cross-sectional area for magnetic flux. This theoretically results in the weakest magnetic reluctance force and thus the lowest restoring torque. Concurrently, the short coil height accommodates the fewest coil turns. The torque generated by the coil is governed by the Lorentz force, expressed as:

$$\tau_{coil} = K_t \cdot I \propto N \cdot B \cdot L \cdot I \tag{2}$$

Where K_t is the torque constant, N is the number of coil turns, B is the magnetic flux density, L is the effective length of the coil, and I is the current. According to Eq.

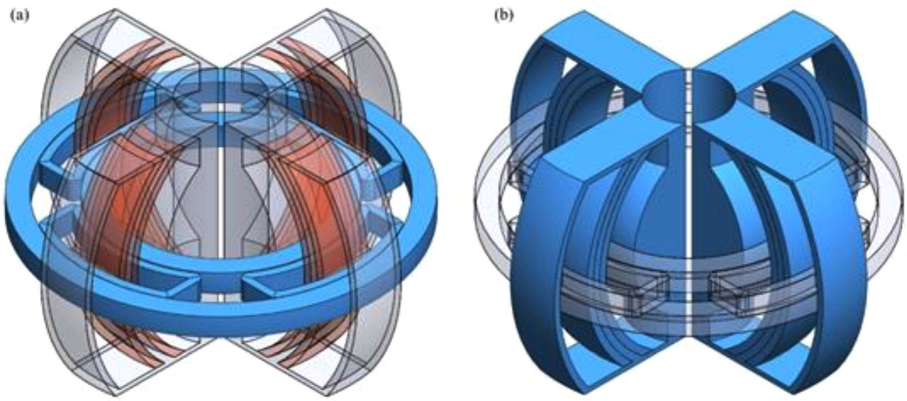

Fig. 5. (Color online) Model for shortest height of both coil and restorative yoke structures (a) stator structure (b) rotor structure.

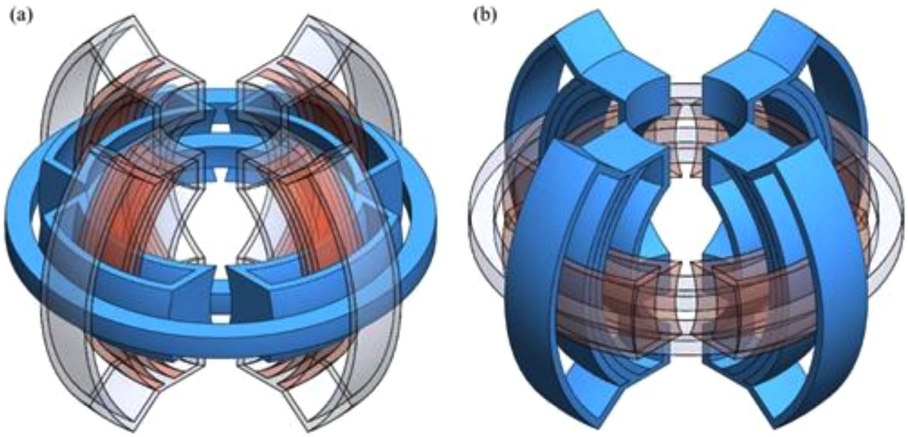

Fig. 6. (Color online) Model for increased height of coil structures (a) stator structure (b) rotor structure.

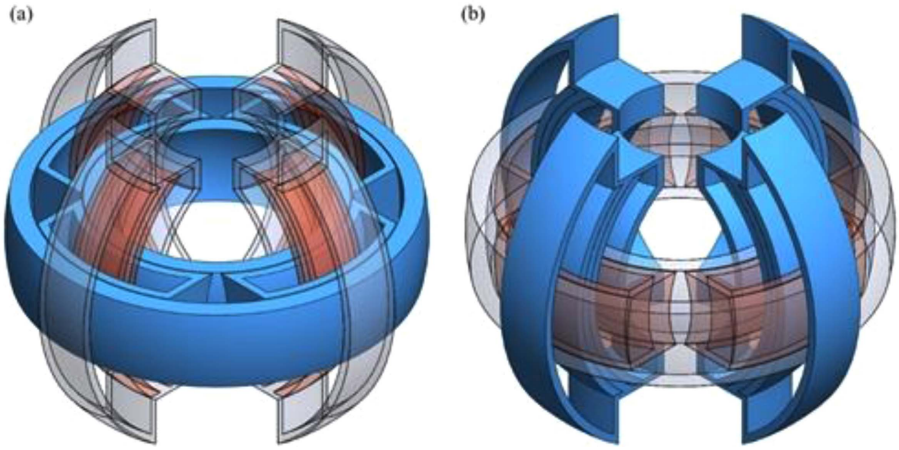

Fig. 7. (Color online) Model for increased height of both coil and restorative yoke structures (a) stator structure (b) rotor structure.

(2), since N is the lowest, this configuration is determined to generate the lowest output torque for a given current.

In Fig. 6, the height of the coil structure is increased while the height of the restorative yoke structure remains unchanged, as shown in Fig. 6(a). This design is anticipated to produce the same restoring torque but a higher output torque when 1 A is applied, as shown in Fig. 7(a). This model is expected to deliver a higher restoring torque and generate the same torque from the coil structure as the model in Fig. 6. The net output torque (τ_{net}) of the motor is the superposition of the propulsive Lorentz torque from the coil (Eq. 2) and the counteractive restoring torque (Eq. 1):

$$\tau_{net} = \tau_{coil} + \tau_r(\theta) = K_t I - K_r \theta \tag{3}$$

Since this model has a significantly higher K_r (a stronger restoring torque), its combined net output torque at any given angle is consequently lower than that of the Fig. 6 model when the same current I is applied.

In the proposed spherical motor design, the coil and restorative yoke structures shown in Figs. 5, 6, and 7(a) are designated as the fixed part (stator), while the magnet structures shown in Figs. 5, 6, and 7(b) are designated as the rotor. Modifications were made to the rotor structure to prevent structural interference when the rotor rotates to 30 degrees. These modifications have a negligible effect on the magnetic circuit. Since the magnetic reluctance of air and copper is at least 1,000 times greater than that of magnetic materials, the impact of the modifications to the yoke length is relatively minor. The increase in magnetic reluctance caused by these adjustments is insignificant compared to the gap between the yokes. Given that the gaps between the yokes remain nearly the same, the magnetic circuit can still be considered to function as originally designed.

4. Design Parameters of Proposed Three Spherical Motor Models

The parameters of the model illustrated in Fig. 5 are shown in Figs. 8-10, with their values listed in Tables 1-3.

The parameters of the model illustrated in Fig. 6 are shown in Figs. 11-13, with their values listed in Tables 4-6.

The parameters of the model illustrated in Fig. 7 are shown in Figs. 14-16, with their values listed in Tables 7-9.

It is important to note that the air gaps in all three models are the same to ensure the magnetic circuits of the three models are similar, as the magnetic reluctance of air is much higher than that of the magnet-conductive materials. Some geometric modifications were applied to the rotor structure in the models of Figs. 6 and 7 to prevent interference between the rotor and stator when the rotor is rotated to 30 degrees, as illustrated in Fig. 17.

Although geometric modifications were applied to the rotor structures in Figs. 6 and 7 to prevent mechanical interference at a 30-degree rotation, the fairness of the performance comparison is strictly maintained. The critical parameters governing the magnetic circuit—specifically the air gap length (G_{air}), magnet dimensions, and the effective overlap area between the coil and magnet—are kept identical across all three models. As

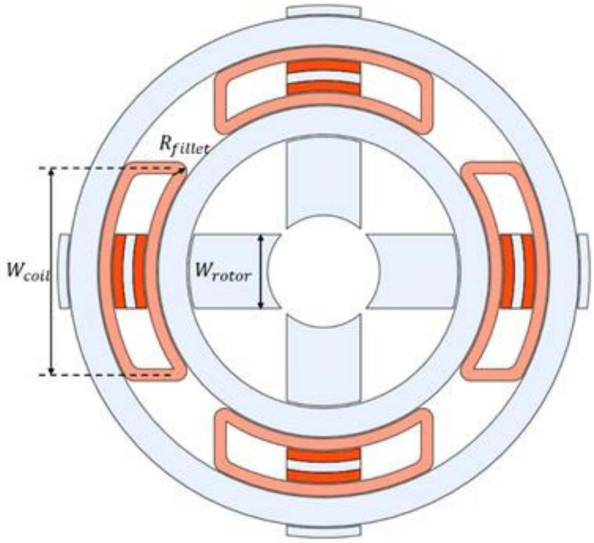

Fig. 10. (Color online) Design parameters of proposed spherical motor: Z-Y cross section of Fig. 5.

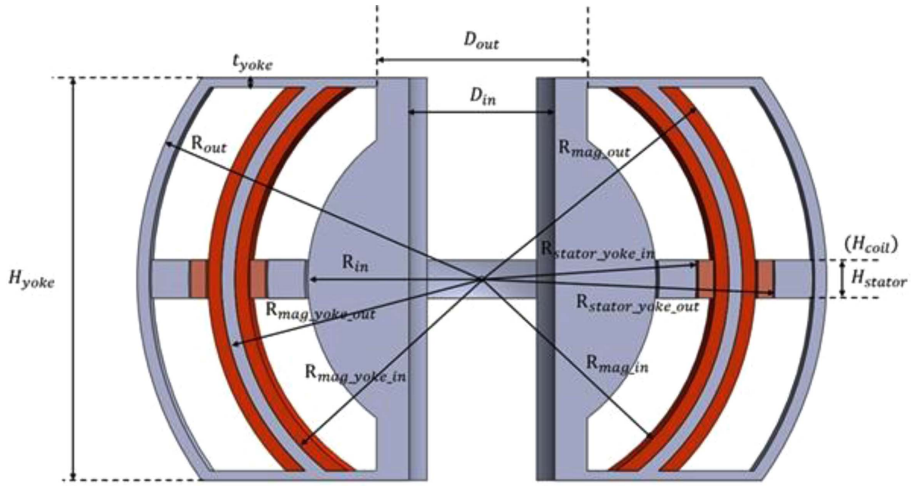

Fig. 8. (Color online) Design parameters of proposed spherical motor: Z-Y cross section of Fig. 5.

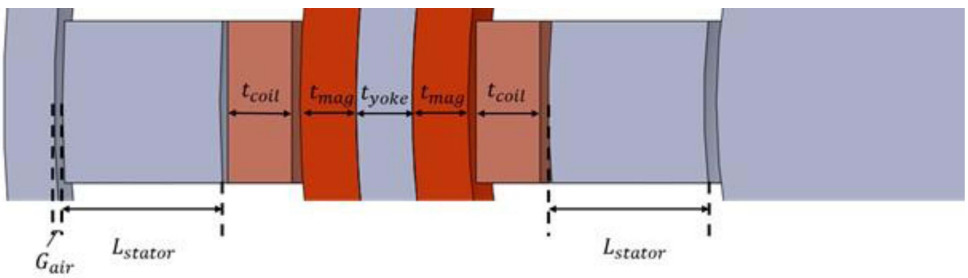

Fig. 9. (Color online) Detail design parameters of proposed spherical motor: Z-Y cross section of Fig. 5.

Table 1. Dimensions values of spherical motor model in Fig. 8.

Symbol	Description	Value
R_{out}	Outer yoke radius	18 mm
R_{in}	Inner yoke radius	9.1 mm
$R_{mag\_yoke\_out}$	Outer radius of yoke attach with magnet	13.6 mm
$R_{mag\_yoke\_in}$	Inner radius of yoke attach with magnet	12.9 mm
t_{yoke}	Thickness of yoke	0.5 mm
H_{yoke}	Height of rotor yoke	21 mm
R_{mag_out}	Outer magnet radius	14.3 mm
R_{mag_in}	Inner magnet radius	12.2 mm
D_{out}	Diameter of outer cylinder structure of rotor	11 mm
D_{in}	Diameter of inner cylinder structure of rotor	7.6 mm
$R_{stator\_yoke\_in}$	Inner stator yoke radius close to magnet	11.2 mm
$R_{stator\_yoke\_out}$	Outer stator yoke radius close to magnet	15.3 mm
H_{stator}	Stator height	2 mm
H_{coil}	Coil height	2 mm

Table 2. Dimension values of spherical motor model in Fig. 9.

Symbol	Description	Value
L_{stator}	Stator yoke length	2 mm
t_{coil}	Coil thickness	0.8 mm
t_{mag}	Magnet thickness	0.7 mm
t_{yoke}	Yoke thickness	0.7 mm
G_{air}	Air gap	0.1 mm

Table 3. Dimension values of spherical motor model in Fig. 10.

Symbol	Description	Value
W_{coil}	Coil width	14 mm
R_{fillet}	Coil fillet's radius	0.7 mm
W_{rotor}	Rotor structure width	5 mm

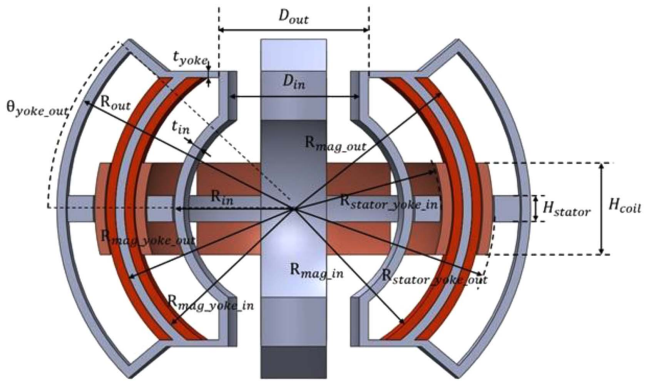

Fig. 11. (Color online) Design parameters of proposed spherical motor: Z-Y cross section of Fig. 6.

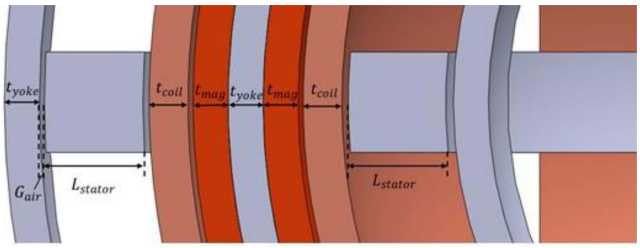

Fig. 12. (Color online) Detail design parameters of proposed spherical motor: Z-Y cross section of Fig. 6.

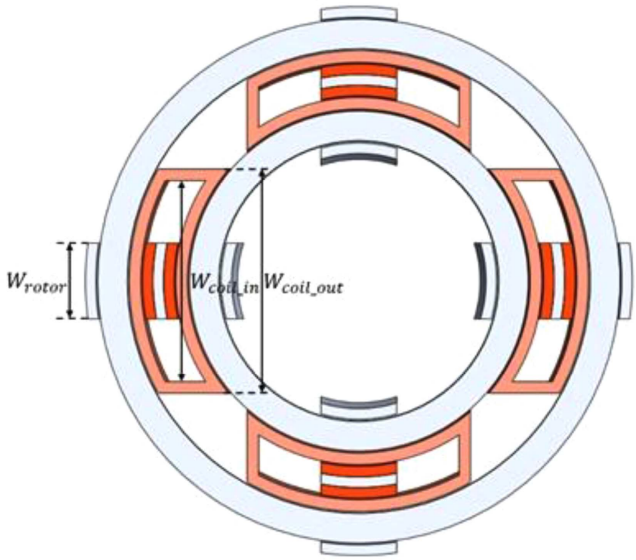

Fig. 13. (Color online) Design parameters of proposed spherical motor: Z-Y cross section of Fig. 6.

Table 4. Dimensions values of spherical motor model in Fig. 11.

Symbol	Description	Value
R_{out}	Outer yoke radius	18.067 mm
R_{in}	Inner yoke radius	9.1 mm
$R_{mag\_yoke\_out}$	Outer radius of yoke attach with magnet	13.6 mm
$R_{mag\_yoke\_in}$	Inner radius of yoke attach with magnet	12.9 mm
t_{yoke}	Thickness of yoke	0.5 mm
t_{in}	Thickness of inner spherical rotor	0.7 mm
q_{yoke_out}	Outer yoke structure angle	40°
R_{mag_out}	Outer magnet radius	14.3 mm
R_{mag_in}	Inner magnet radius	12.2 mm
$R_{stator\_yoke\_in}$	Inner stator yoke radius close to magnet	11.2 mm
$R_{stator\_yoke\_out}$	Outer stator yoke radius close to magnet	15.3 mm
D_{out}	Diameter of outer cylinder structure of rotor	11.4 mm
D_{in}	Diameter of inner cylinder structure of rotor	10 mm
H_{stator}	Stator height	2 mm
H_{coil}	Coil height	7 mm

Table 5. Dimension values of spherical motor model in Fig. 12.

Symbol	Description	Value
L_{stator}	Stator yoke length	2 mm
t_{coil}	Coil thickness	0.775 mm
t_{mag}	Magnet thickness	0.7 mm
t_{yoke}	Yoke thickness	0.7 mm
G_{air}	Air gap	0.1 mm

Table 6. Dimension values of spherical motor model in Fig. 13.

Symbol	Description	Value
W_{coil_out}	Outer coil width	14.75 mm
W_{coil_in}	Inner coil width	13.25 mm
W_{rotor}	Rotor structure width	5 mm

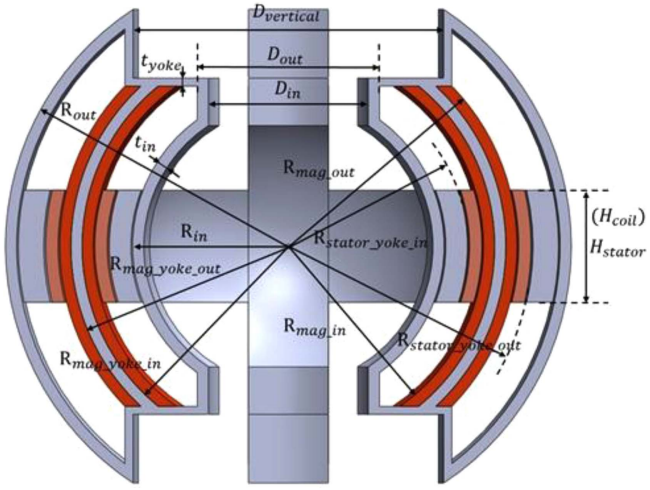

Fig. 14. (Color online) Design parameters of proposed spherical motor: Z-Y cross section of Fig. 7.

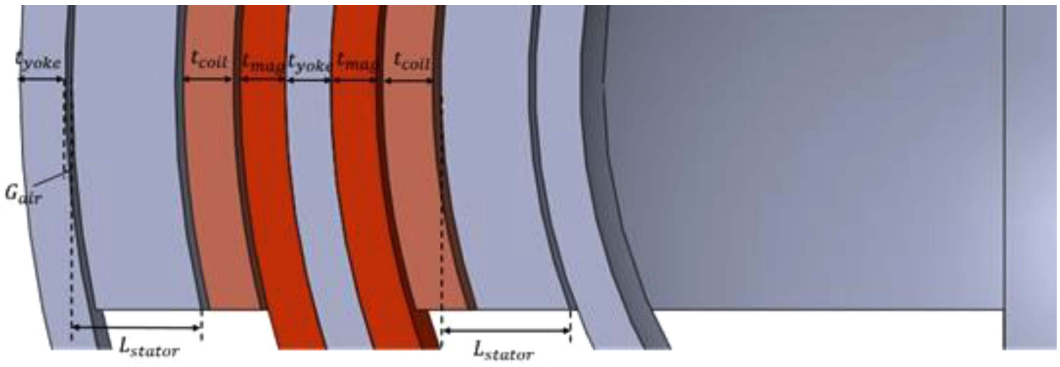

Fig. 15. (Color online) Detail design parameters of proposed spherical motor: Z-Y cross section of Fig. 7.

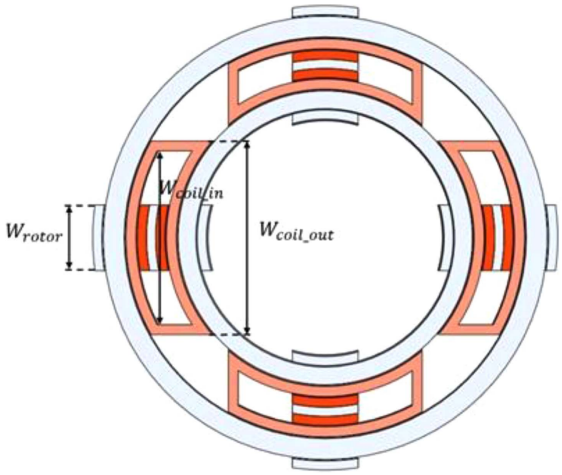

Fig. 16. (Color online) Design parameters of proposed spherical motor: Z-Y cross section of Fig. 7.

Table 8. Dimension values of spherical motor model in Fig. 15.

Symbol	Description	Value
L_{stator}	Stator yoke length	2 mm
t_{coil}	Coil thickness	0.775 mm
t_{mag}	Magnet thickness	0.7 mm
t_{yoke}	Yoke thickness	0.7 mm
G_{air}	Air gap	0.1 mm

Table 9. Dimension values of spherical motor model in Fig. 16.

Symbol	Description	Value
W_{coil_out}	Outer coil width	14.75 mm
W_{coil_in}	Inner coil width	13.25 mm
W_{rotor}	Rotor structure width	5 mm

Table 7. Dimension values of spherical motor model in Fig. 14.

Symbol	Description	Value
R_{out}	Outer yoke radius	17.69 mm
R_{in}	Inner yoke radius	9.74 mm
$R_{mag\_yoke\_out}$	Outer radius of yoke attach with magnet	13.6 mm
$R_{mag\_yoke\_in}$	Inner radius of yoke attach with magnet	12.9 mm
t_{yoke}	Thickness of yoke	0.5 mm
t_{in}	Thickness of inner spherical rotor	0.7 mm
R_{mag_out}	Outer magnet radius	14.3 mm
R_{mag_in}	Inner magnet radius	12.2 mm
$R_{stator\_yoke\_in}$	Inner stator yoke radius close to magnet	11.2 mm
$R_{stator\_yoke\_out}$	Outer stator yoke radius close to magnet	15.3 mm
D_{out}	Diameter of outer cylinder structure of rotor	11.4 mm
D_{in}	Diameter of inner cylinder structure of rotor	10 mm
$D_{vertical}$	Diameter of vertical cylinder structure of rotor	19.4 mm
H_{stator}	Stator height	7 mm
H_{coil}	Coil height	7 mm

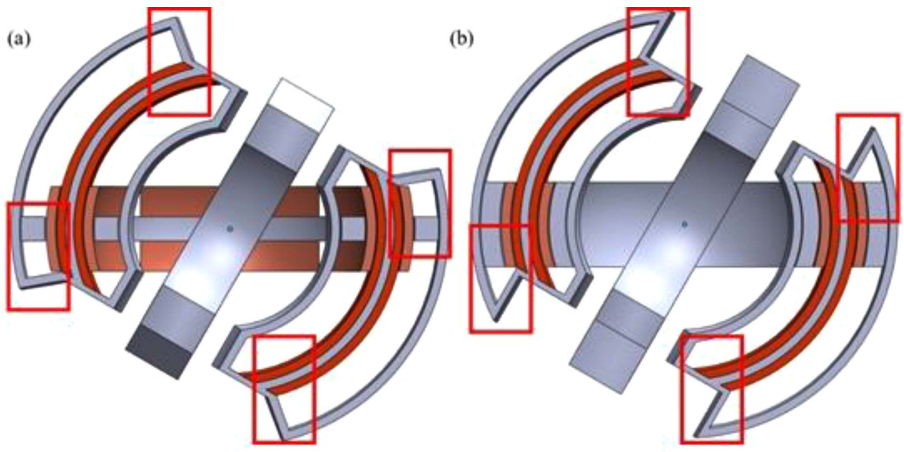

Fig. 17. (Color online) Illustration of rotor structure design to avoid interference.

mentioned in Section 3, the material removed for clearance is located in a region of low magnetic flux density. Since the total reluctance of the magnetic circuit is dominated by the air gap (which remains constant), the minor variations in the yoke geometry have a negligible impact on the magnetic flux generation. Therefore, the observed performance differences can be attributed solely to the intended design variables: the coil height and the restorative yoke height.

5. Maxwell Magnetic Simulation Setup

The simulation was conducted using the ANSYS Maxwell 3D finite element analysis (FEA) solver. The yoke material was set as SS41 steel, with its measured BH curve (averaged from the first and fourth quadrants) as shown in Fig. 18(a). The magnet material was set as N42M at 20°C from the default database, and the coil material was set as copper. To accurately model an open-space environment, a Region was created using a 200% Percentage Offset from the model's bounding box, and its Boundary property was set with default Neumann boundary conditions (Zero Tangential H-field). The simulation was excited by applying current to the coils, and the rotor torque was calculated as it rotated in the positive X-axis direction (Fig. 4).

To ensure simulation accuracy and convergence, an Adaptive Mesh Refinement strategy was employed. The adaptive process was configured to converge when the Percent Error between iterations fell below 0.7%, with a Maximum Number of Passes set to 20. The Refinement Per Pass was set to 30%. For the solver, the Nonlinear Residual was set to 0.001 to accurately handle the non-linear SS41 material properties, and the Relative Residual for the matrix solver was set to 1e-06.

Furthermore, to accurately calculate the magnetic forces, a Length Based mesh operation (mesh seeding) was applied directly to the faces defining the 0.1 mm air gap, restricting the maximum element length in this critical region to 0.05 mm. A coarser length-based mesh (e.g., 2.95 mm) was applied to the bulk yoke components to manage the overall element count. Since the structure is symmetrical, the torque generated in the opposite direction is assumed to be equal in magnitude but opposite in direction. The resulting magnetic field plot (Fig. 18(b)) confirms the field direction closely resembles the intended magnetic circuit design.

6. Simulation Results and Discussion

The simulation results for each model excited with current are illustrated in Figs. 19-21. From Figs. 19-21(a), it can be seen that when no current is applied, the torque curve in the X-axis direction (GX torque at 0A) nearly intersects the horizontal line at 0 mN·m, with the X value being opposite to the Y value. This indicates that when the rotor is at a negative angle, the torque generated by the attraction between the permanent magnet and the restorative yoke structure will force the rotor to rotate back to the 0-degree position. The same effect occurs when the rotor is at a positive angle, demonstrating that the magnetic circuit provides a restoring torque that brings the rotor back to the level position. Furthermore, from Figs. 19-21, the torque curves in the Y and Z-axis directions approach zero, regardless of the current applied. This suggests that no torque is generated in these directions when the rotor is forced to rotate to a positive angle or when no current is input. This indicates that the spherical motor design enables independent rotational movement.

However, the results also indicate that it is possible for the rotor to fail to achieve a 30-degree rotation when 1A (the design's maximum current) is applied, generating a 24At magnetic field. This is because the restoring torque is stronger than the Lorentz torque, as shown in Fig. 19(a). The torque curve in the X-axis direction for 24At

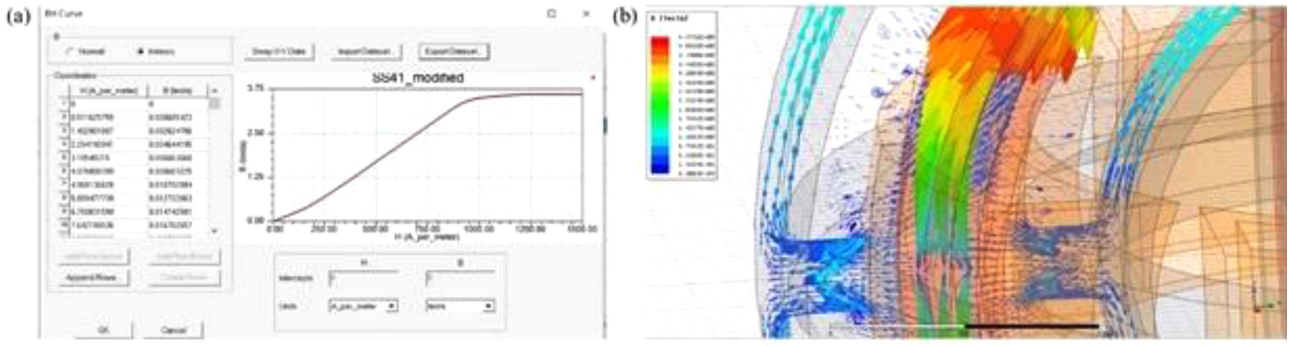

Fig. 18. (Color online) (a) Initial BH curve of SS41 steel (b) B vector plot.

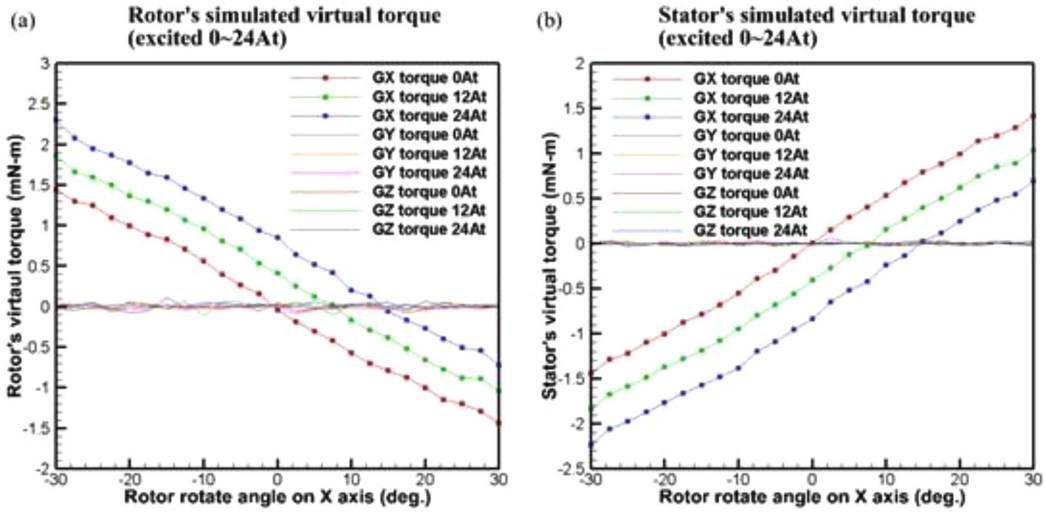

Fig. 19. (Color online) Simulation torque results for Fig. 5 model (a) rotor (b) stator.

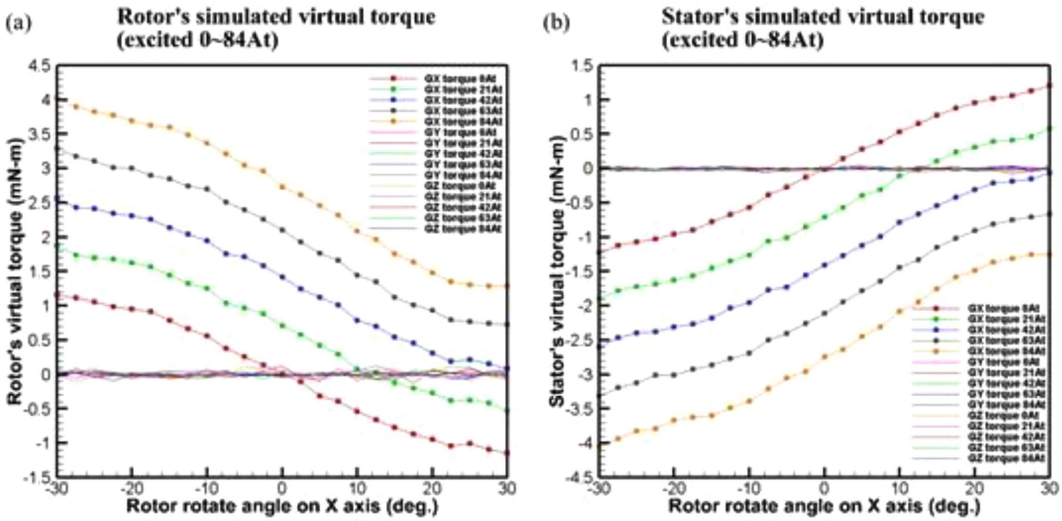

Fig. 20. (Color online) Simulation torque results for Fig. 6 model (a) rotor (b) stator.

intersects the 0 mN·m line before the rotor reaches 30 degrees, indicating that a balance angle is achieved before the rotor completes the desired rotation. Nevertheless, the results show that the model in Fig. 6, which has a modified coil structure with more turns to enhance its total magnetic field energy, generates greater torque when 1A is applied. This allows the rotor to achieve a 30-degree rotation, demonstrating that increasing the coil structure's size can boost the total generated torque. Similarly, Fig. 21 (the results of the model in Fig. 7) shows that enhancing both the coil and restorative torque allows the goal of a 30-degree rotation to be achieved. Based on the simulation results, the proposed model in Fig. 6 is a suitable design as it requires less current to achieve a 30-degree rotation.

From Figs. 19-21, the torque curve in the X-axis direction when no current is input exhibits high linearity. This indicates that the restoring torque is highly linear with respect to the rotated angle. Additionally, since the torque curve in the X-axis direction shifts upward when the coil is excited, it demonstrates that the restoring torque characteristic is not affected by the magnetic field generated by the current. From Figs. 19 and 21, the gaps between the torque curves in the X-axis direction for different current inputs remain nearly constant. This shows that the output torque generated by the coil adds a consistent magnitude of torque as the current increases. The linear relationship between current and output torque is expected, as the driving force is Lorentz force, which inherently has a linear relationship with current magnitude.

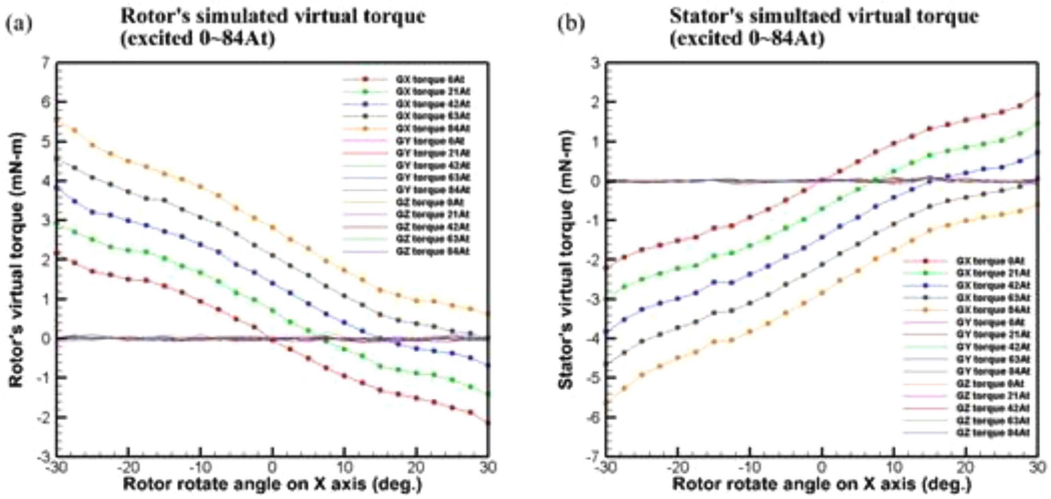

Fig. 21. (Color online) Simulation torque results for Fig. 7 model (a) rotor (b) stator.

Furthermore, the parallel nature of the torque curves in the X-axis direction for different current inputs indicates that the current-generated torque has a small rate of change with respect to the rotor angle.

7. Conclusion

This study proposed and validated a novel two-degree-of-freedom voice coil spherical motor. Through simulation, the design was confirmed to possess several key characteristics: a highly linear restoring torque that functions like a magnetic spring, independent rotational control, and a maximum working angle of ±30 degrees. The verification of these features confirms the design's potential for high-precision position control and its adaptability for various load requirements.

As shown in Table 10, the proposed design achieves a moderate torque constant (4.02 mN·m/A), which is suitable for low-current applications that require high precision. While the Kim *et al.* [17] (2013) design and the Heya *et al.* [22] (2022) design offer larger torque constants (0.35 N·m/A and 8-12 mN·m/A, respectively), the proposed design's main strength lies in its efficiency and compact size while still offering linear passive restoring torque. This makes the design particularly effective in precision applications where low-power operation and stable positioning are essential.

Despite these promising simulation results, this study has several limitations. First, the findings are based purely on electromagnetic simulations using ANSYS Maxwell. Factors such as friction, manufacturing tolerances, and assembly errors, which will be present in a physical system, were not considered. Second, the thermal analysis of the coil structure under continuous current excitation was not performed. The heat generated (Joule heating) could potentially affect the performance of the N42M permanent magnets. Finally, the current design in Fig. 5 model was unable to reach the full 30-degree angle at 1A, indicating that the balance between restoring torque and Lorentz torque requires further optimization for low-current applications.

Future work will focus on addressing these limitations. The primary objective is the fabrication and experimental validation of a physical prototype, focusing on the Fig. 6 model which showed the most balanced performance. A test rig will be developed to measure the output torque and restoring torque characteristics, allowing for direct comparison with the simulation data presented in Figs.

Table 10. Quantitative Comparison with Existing Voice Coil Spherical Actuators.

Parameter	Proposed Design (Fig. 6 model)	Kim *et al.* [17] (2013)	Heya *et al.* [22] (2022)
Degree of Freedom	2-DOF	2-DOF	3-DOF
Outer Dimensions	ϕ36.1 mm	ϕ100 mm	ϕ30 mm
Max. Working Angle	± 30°	± 40°	± 20°
Tilt Torque Constant (For X, Y Axes)	4.02 mN·m/A	0.35 N·m/A	8~12 mN·m/A
Passive Restoring Torque	Yes (highly linear)	No	No

19-21. Furthermore, a closed-loop control system based on this model will be developed to investigate its practical positioning accuracy and dynamic response. We will also explore the potential of extending this validated magnetic circuit design to a 3-DOF spherical motor, as discussed in the introduction.

The unique characteristics of this design, particularly its passive linear restoring torque and independent axis control, make it highly suitable for applications requiring precision pointing and stable centering. Potential applications include robotic eyes or camera stabilization gimbals (where the restoring force provides stability against vibrations), LiDAR or laser beam steering systems (requiring fast and precise 2-DOF tilting), and haptic feedback devices.

Funding: This study was funded by the National Science and Technology Council of Taiwan under Grant Nos. NSTC 110-2221-E-006-162-MY2.

Acknowledgments

Ansys Inc. is thanked for providing ANSYS academic partner program.

References

[1] U. Yongsu, T. Yano, 2009 International Conference on Mechatronics and Automation (2009) pp. 170-175.
[2] L. Yan, I. M. Chen, C. K. Lim, G. Yang, W. Lin, and K.-M. Lee, IEEE/ASME Transactions on Mechatronics **13**, 239 (2008).
[3] J. He, G. Li, R. Zhou, and Q. Wang, IEEE Trans. Magn. **56**, 1 (2020).
[4] Q. Chen, X. Yang, G. Zhong, B. Zeng, S. Zhao, and J. Cao, IEEE Trans. Magn. **58**, 1 (2022).
[5] L. Yan, Y. Liu, L. Zhang, Z. Jiao, and C. Gerada, IEEE Trans. Ind. Electr. **66**, 9112 (2019).
[6] L. Gan, Y. Pei, and F. Chai, IEEE Trans. Ind. Electr. **67**, 421 (2020).
[7] M. Kumagai and R. L. Hollis, 2013 IEEE International Conference on Robotics and Automation (2013) pp. 1528-1533.
[8] L. Yuan, J. Zhang, S.-L. Chen, Y. Liang, J. Chen, C. Zhang, and G. Yang, Energies **12**, 1553 (2019).
[9] B. Dehez, G. Galary, D. Grenier, and B. Raucent, IEEE Trans. Magn. **42**, 2077 (2006).
[10] J. F. P. Fernandes, S. M. Vieira, and P. J. Costa Branco, IEEE Transactions on Energy Conversion **33**, 660 (2018).
[11] M. Shi, Q. Wang, G. Li, J. Xu, Q. Han, and Q. Ye, IEEE Transactions on Industrial Electronics **70**, 6099 (2023).
[12] K.-M. Lee, R. B. Roth, and Z. Zhou, J. Dyn. Syst. Measurement, and Control **118**, 29 (1996).
[13] W. Tao, G. Li, L. Ju, R. Zhou, and C. Hu, 2018 IEEE International Power Electronics and Application Conference and Exposition (PEAC) (2018) pp. 1-6.
[14] S. Toyama, S. Sugitani, G. Zhang, Y. Miyatani, and K. Nakamura, Proceedings of 1995 IEEE International Conference on Robotics and Automation (1995) pp. 2935-2940
[15] R. Takehana, H. Paku, and K. Uchiyama, 2016 7th International Conference on Mechanical and Aerospace Engineering (ICMAE) (2016) pp. 352-357.
[16] F. Wang, U. Nishizawa, H. Tanaka, and S. Toyama, Journal of Vibroengineering **20**, 2939 (2018).
[17] H. Kim, H. Kim, D. Ahn, and D. Gweon, Sensors and Actuators A: Physical **203**, 181 (2013).
[18] H.Y. Kim, H. Kim, D.-G. Gweon, and J. Jeong, IEEE/ASME Transactions on Mechatronics **20**, 532 (2015).
[19] A. Heya, K. Hirata, and N. Niguchi, IEEE Trans. Magn. **54**, 1 (2018).
[20] A. Heya, Y. Nakata, H. Ishiguro, and K. Hirata, 2020 International Conference on Electrical Machines (ICEM) (2020) pp. 735-740.
[21] S. Kuribayashi, A. Heya, K. Hirata, and M. Kurita, 2021 24th International Conference on Electrical Machines and Systems (ICEMS) (2021) pp. 79-82.
[22] A. Heya and K. Hirata, Sensors **22**, 6926 (2022).
[23] Y. Tamaki, A. Heya, and T. Inoue, IEEE Trans. Magn. **59**, 1 (2023).